# Transient and Numerical Models of Three-Phase Induction Motor

Vasilija Sarac, Goce Stefanov
Faculty of Electrical Engineering
University Goce Delchev
Stip, Macedonia
vasilija.sarac@ugd.edu.mk , goce.stefanov@ugd.edu.mk

Neven Trajchevski
Military Academy Skopje
University Goce Delchev
Stip, Macedonia
neven.trajchevski@ugd.edu.mk

*Abstract*— **The two different mathematical models of three-phase induction motor are derived in order to estimate the motor dynamic behavior during acceleration in different operating modes. The first model is derived from a set of differential equations applied and solved in Simulink. The second model and its set of differential equations are solved using numerical methods in Matlab. The analytical calculation, the experiment, the Finite Element Method (FEM) and the motor model in PSIM software verify the results of both motor transient models. The FEM motor model allows calculation of the magnetic flux density distribution in the motor's cross-section and in the air gap. Additionally, the torque is calculated in the FEM model for different operating speeds and its value is compared with the previously obtained results from the transient models.**

***Keywords- Induction motor, dynamic models, transient characteristics, FEM model.***

## I. INTRODUCTION

The three-phase induction motors are among the most widespread induction motors in industrial applications. Since Tesla's invention of the polyphase induction motor and his experimental proof that induction motors can be made with a high degree of efficiency, the three-phase induction motor has become an irreplaceable part in the system of electricity utilization [1]. Its application is significantly improved with the use of power converters and digital controllers allowing motor operation in variable speed applications and complex control systems [2]-[4]. The assessment of motor coupling with the load and its transient behavior during acceleration, as well as during steady-state operation is one of the most important engineering tasks. Various simulation transient models of single and three-phase induction motors can be observed in the literature [5]-[8]. In addition, transient behavior of the motor is modeled and analyzed in cases when the motor is coupled with a soft starter [9]-[10]. Usually, these models are based on one general transformation, which eliminates all time-varying inductances in the electrical machine by referring the stator and rotor variables to a frame of reference, which may rotate at any angular velocity or remain stationary. All known transformations may be obtained by simply assigning the appropriate speed of rotation to this so-called arbitrary reference frame. In this paper, two different transient models of the motor, allowing evaluation of motor dynamic behavior during acceleration, are derived. The first one is defined with a set of five differential equations, modeled and solved in Simulink. This model is referred to as the simulation model (SM). The second one and its set of differential equations is solved by using numerical methods in Matlab, and this model is referred to as the numerical model (NM). The motor speed and electromagnetic torque as time dependent variables are obtained from both transient motor models. The obtained results are related to various operating modes such as the no load or rated load. The verification of the obtained results from both motor transient models is done by comparison with the results from the motor analytical model, experiments, the FEM model of the motor and motor model in PSIM software. The motor model in PSIM software allows direct comparison of transient characteristics of speed, current and torque from SM and NM with the transient characteristics obtained from the PSIM software. The FEM model of the motor is derived in order to have a clear overview of the magnetic flux distribution in the motor cross-section, as well as in the motor air gap. It allows assessment of the machine core saturation due to the high flux density. The core saturation has a significant influence on the motor's proper operation due to increased losses and motor overheating. Furthermore, as an output from the FEM model, the motor torque is calculated at various operating modes. The obtained values of torque from the FEM models are compared with the obtained torque from the adequate transient characteristics in order to verify the accuracy of the transient models. This paper presents an analysis of the three-phase squirrel cage motor with rated data: output power 2.2 kW, rated speed 1410 rpm, supply voltage 380/220 V in Y/Δ winding connection and rated current of 8.7/5.5 A.

## II. TRANSIENT MOTOR MODELS

### A. Simulation Model-Methodology

The first step in mathematical modeling of the transient motor model in Simulink is to transform the supply voltages from the three-phase system (a, b, c) into the synchronously rotating d, q system. The transformation equations are:

$$U_{ds} = -\frac{1}{\sqrt{3}}\left(U_b - U_c\right)\cos\theta + U_a \sin\theta \qquad (1)$$

$$U_{qs} = \frac{1}{\sqrt{3}}\left(U_b - U_c\right)\sin\theta + U_a \cos\theta \qquad (2)$$

Where $\omega = \frac{d\theta}{dt}$ i.e. angular displacement $\theta = \int_0^t \omega dt$ . The voltages $U_a$, $U_b$ and $U_c$ are the three-phase supply voltages at 220 V, 50 Hz. The variable ω is associated to the frequency of the supply voltage of the motor. In case of symmetrical three-phase supply voltage ω=314 rad/s. The voltage equations of the stator and rotor circuits are:

$$U_{qs} = R_s i_{qs} + \omega\psi_{ds} + \frac{d\psi_{qs}}{dt} \tag{3}$$

$$U_{ds} = R_s i_{ds} - \omega\psi_{qs} + \frac{d\psi_{ds}}{dt} \tag{4}$$

$$0 = R_r i_{qr} + (\omega - \omega_r)\psi_{dr} + \frac{d\psi_{qr}}{dt} \tag{5}$$

$$0 = R_r i_{dr} - (\omega - \omega_r)\psi_{qr} + \frac{d\psi_{dr}}{dt} \tag{6}$$

In (5) and (6) the transformed rotor voltages $U_{qr}$ and $U_{dr}$ are considered to be equal to zero, since the rotor winding is of the squirrel cage type, and consequently it is short circuited. In the above equations, $\omega_r$ is the rotor angular velocity and ω is the arbitrary angular speed, which depends on the frequency of the voltage supply. The flux linkages of the stator and rotor circuits are defined as:

$$\psi_{qs} = L_s i_{qs} + L_{sr} i_{qr} \tag{7}$$

$$\psi_{ds} = L_s i_{ds} + L_{sr} i_{dr} \tag{8}$$

$$\psi_{qr} = L_r i_{qr} + L_{sr} i_{qs} \tag{9}$$

$$\psi_{dr} = L_r i_{dr} + L_{sr} i_{ds} \tag{10}$$

All variables related to the stator have the subscript "*s*", and those related to the rotor have the subscript "*r*'. $R_s$ and $R_r$ are the stator and rotor resistances, $L_s$ and $L_r$ are the stator and rotor inductances, and $L_{sr}$ is the mutual inductance between the stator and rotor winding. By expressing the stator currents $i_{qs}$ and $i_{ds}$ from (7) and (8) and their replacement into (9) and (10), the following equations are obtained:

$$\psi_{qr} = L_r i_{qr} + L_{sr}\left(\frac{\psi_{qs}}{L_s} - \frac{L_{sr}}{L_s} i_{qr}\right) \tag{11}$$

$$\psi_{dr} = L_r i_{dr} + L_{sr}\left(\frac{\psi_{ds}}{L_s} - \frac{L_{sr}}{L_s} i_{dr}\right) \tag{12}$$

By replacing (11) and (12) into (5) and (6) and integrating over time:

$$i_{qr} = \frac{L_s R_r}{L_{sr}^2 - L_s L_r}\int_0^t i_{qr}dt - \omega\int_0^t i_{dr}dt + \frac{L_{sr}\omega}{L_{sr}^2 - L_s L_r}\int_0^t \psi_{ds}dt + \int_0^t \omega_r i_{dr}dt - \frac{L_{sr}}{L_{sr}^2 - L_s L_r}\int_0^t \omega_r \psi_{ds}dt + \frac{L_{sr}}{L_{sr}^2 - L_s L_r}\psi_{qs} \tag{13}$$

$$i_{dr} = \frac{L_s R_r}{L_{sr}^2 - L_s L_r}\int_0^t i_{dr}dt + \omega\int_0^t i_{qr}dt - \frac{L_{sr}\omega}{L_{sr}^2 - L_s L_r}\int_0^t \psi_{qs}dt - \int_0^t \omega_r i_{qr}dt + \frac{L_{sr}}{L_{sr}^2 - L_s L_r}\int_0^t \omega_r \psi_{qs}dt + \frac{L_{sr}}{L_{sr}^2 - L_s L_r}\psi_{ds} \tag{14}$$

The flux linkages $\psi_{ds}$ and $\psi_{qs}$ can be expressed from the transformed voltages $U_{ds}$ and $U_{qs}$. By replacing the currents $i_{qs}$ and $i_{ds}$ from the equations (7) and (8) in (3) and (4), rearranging the equations per flux linkages and their integration over time, the following equations are obtained:

$$\psi_{qs} = \int_0^t U_{qs}dt - \frac{R_s}{L_s}\int_0^t \psi_{qs}dt + \frac{L_{sr}R_s}{L_s}\int_0^t i_{qr}dt - \omega\int_0^t \psi_{ds}dt \tag{15}$$

$$\psi_{ds} = \int_0^t U_{ds}dt - \frac{R_s}{L_s}\int_0^t \psi_{ds}dt + \frac{L_{sr}R_s}{L_s}\int_0^t i_{dr}dt + \omega\int_0^t \psi_{qs}dt \tag{16}$$

The equations (1), (2), (13), (14), (15) and (16) together with the equation, which defines the rotor speed, constitute the motor transient model. The equation of the rotor speed is:

$$\omega_r = \frac{6L_{sr}}{JL_s}\int_0^t \psi_{qs} i_{dr}dt - \frac{6L_{sr}}{JL_s}\int_0^t \psi_{ds} i_{qr}dt - \frac{2}{J}\int_0^t M_s dt \tag{17}$$

$M_s$ [Nm]-is the load torque and J [$kgm^2$] is the moment of inertia of the motor. The rotor currents and flux linkages are expressed with integral equations instead of differential, as Simulink has more stability in convergence of the solution when equations are expressed in integral form. The electromagnetic torque is found from:

$$M_{em} = \left(\frac{3}{2}\right)\left(\frac{P}{2}\right)L_{sr}\left(\frac{\psi_{qs}}{L_s} i_{dr} - \frac{\psi_{ds}}{L_s} i_{qr}\right) \tag{18}$$

P is the number of poles of the motor. The presented equations (1), (2), (13), (14), (15), (16), (17) and (18) are solved in Simulink for Matlab. As an output, the electromagnetic torque-$M_{em}$ and rotor speed-$\omega_r$ as time dependent variables are obtained from the simulation model for different operating regimes: no-load, and rated load of 14 Nm. Beside this, the transient characteristics of the stator current are available as an output from this simulation model. The stator currents are obtained from the inverse transformation from the d,q system into the three-phase a, b, c system.

$$i_a = i_{qs}\cos\theta + i_{ds}\sin\theta \tag{19}$$

$$i_b = \left(-\frac{1}{2}i_{qs} - \frac{\sqrt{3}}{2}i_{ds}\right)\cos\theta + \left(\frac{\sqrt{3}}{2}i_{qs} - \frac{1}{2}i_{ds}\right)\sin\theta \quad (20)$$

$$i_c = \left(-\frac{1}{2}i_{qs} + \frac{\sqrt{3}}{2}i_{ds}\right)\cos\theta - \left(\frac{\sqrt{3}}{2}i_{qs} + \frac{1}{2}i_{ds}\right)\sin\theta \quad (21)$$

*B. Simulation Model-Results*

The transient characteristics of speed and torque at no load and rated load are presented in Figs. 1 and 2, respectively. Fig. 3 presents the transient characteristics of the stator current for no load and rated load.

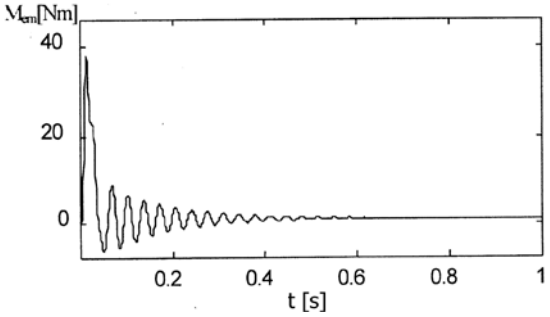


(a) no-load

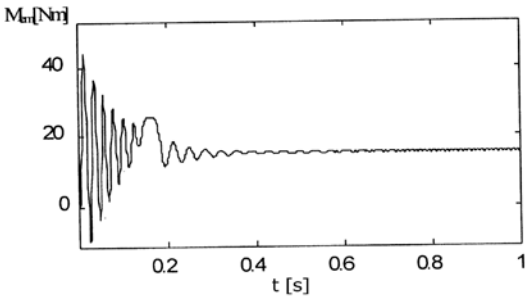


(b) rated load

Figure 6. Transient characteristics of torque

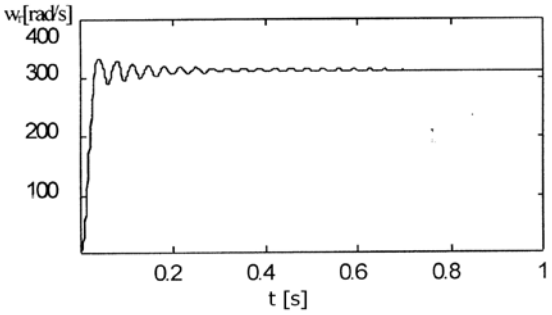


(a) no-load

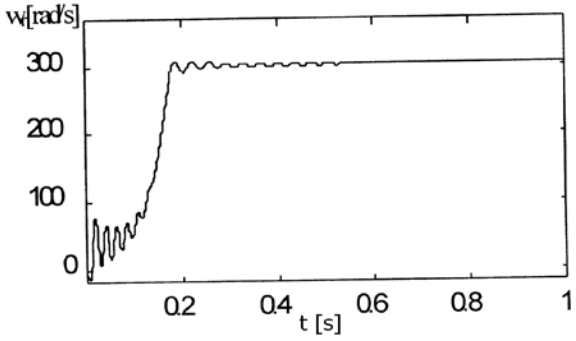


(b) rated load

Figure 7. Transient characteristics of speed

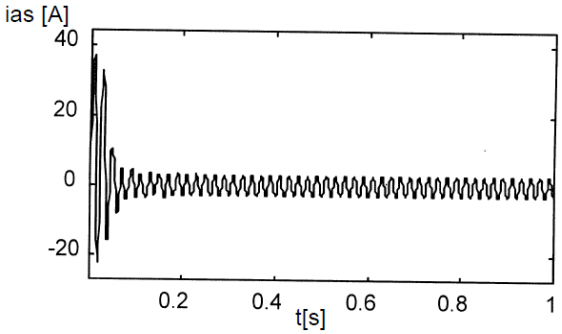


(a) no-load

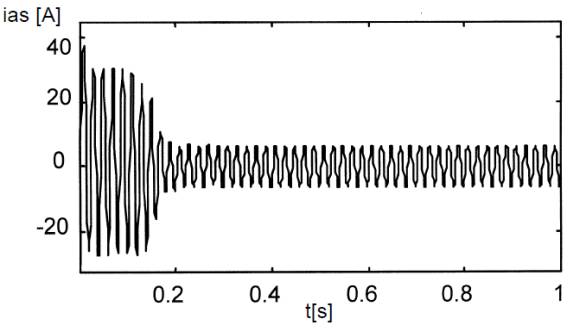


(b) rated load

Figure 8. Transient characteristics of current

*C. Numerical Model-Methodology*

The motor numerical model consists of a set of five differential equations in which the time-dependent variables (flux linkages and speed) are transformed in the stationary reference frame or α, β reference frame. The differential equations are:

$$\frac{d\psi_{s\alpha}}{dt} = \sqrt{2}U_{nf}\cos\omega t - a_1\psi_{s\alpha} + a_2\psi_{r\alpha} \quad (22)$$

$$\frac{d\psi_{s\beta}}{dt} = \sqrt{2}U_{nf}\cos\omega t - a_1\psi_{s\beta} + a_2\psi_{r\beta} \quad (23)$$

$$\frac{d\psi_{r\alpha}}{dt} = a_3\psi_{s\alpha} - a_4\psi_{r\alpha} - \omega_r\psi_{r\beta} \quad (24)$$

$$\frac{d\psi_{r\beta}}{dt} = a_3\psi_{s\beta} - a_4\psi_{r\beta} + \omega_r\psi_{r\alpha} \quad (25)$$

$$\frac{d\omega_r}{dt} = P(M_{em} - M_s)/J \quad (26)$$

$$M_{em} = a_5\left(\psi_{s\beta}\psi_{r\alpha} - \psi_{r\beta}\psi_{s\alpha}\right) \quad (27)$$

$$a_1 = \frac{R_s L_r}{L_s L_r - L_{sr}^2} \quad a_2 = \frac{R_s L_{sr}}{L_s L_r - L_{sr}^2} \quad a_3 = \frac{R_r L_s}{L_s L_r - L_{sr}^2} \quad (28)$$

$$a_4 = \frac{R_r L_{sr}}{L_s L_r - L_{sr}^2} \quad a_5 = \frac{PL_{sr}}{L_s L_r - L_{sr}^2} \quad (29)$$

The equations (22)÷(27) are solved in Matlab with the Runge Kutta solver, giving as an output the transient characteristics of torque and speed.

*D. Numerical Model-Results*

The electromagnetic torque and motor speed, as time dependent variables, are obtained from the motor numerical models. The transient characteristics of speed and torque for various operating modes are presented in Figs. 4 and 5 respectively.

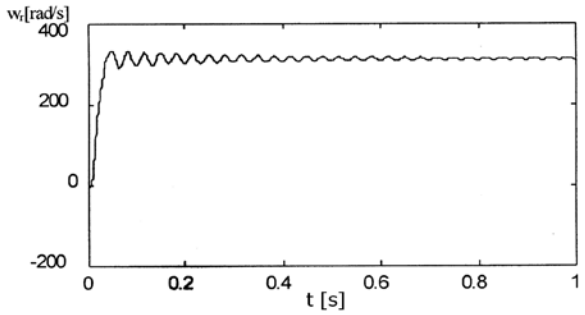


(a) no-load

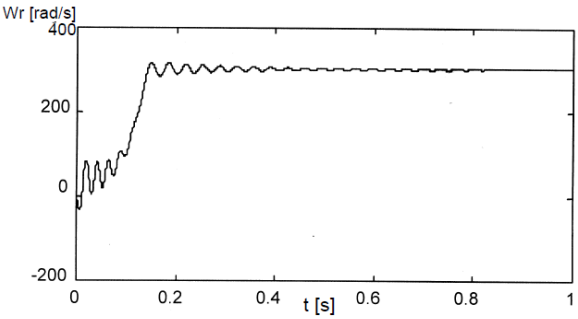


(b) rated load

Figure 9. Transient characteristics of speed

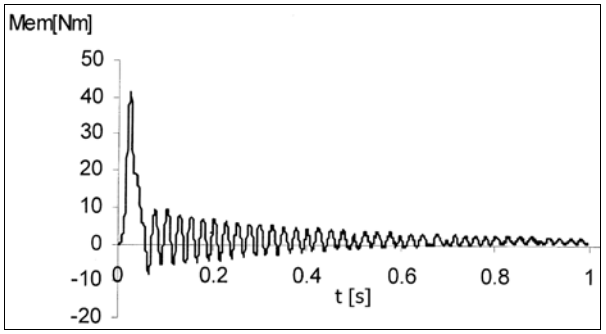


(a) no-load

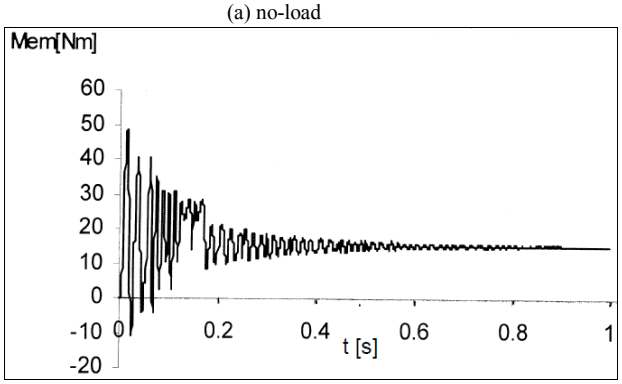


(b) rated load

Figure 10. Transient characteristics of torque

## III. FEM MODEL

The Finite Element Method belongs to the numerical techniques often used for calculating various electromagnetic quantities. Over the last years, it has proven to be a reliable tool in designing machines as well as in terms of the magnetic flux density calculation in the entire cross-section of the analyzed machine allowing points of magnetic core with high flux density to be detected [11]-[14]. The knowledge of the magnetic flux density distribution in the machine cross-section gives the possibility of redesigning or optimizing the machine design, which leads to more efficient electrical machines with decreased losses and electricity consumption [15]-[17]. The flux density **B** is calculated from the magnetic vector potential **A**. In order Maxwell equations to be solved, the complete machine cross-section is divided in numerous elements forming the mesh of finite elements (Fig. 6).

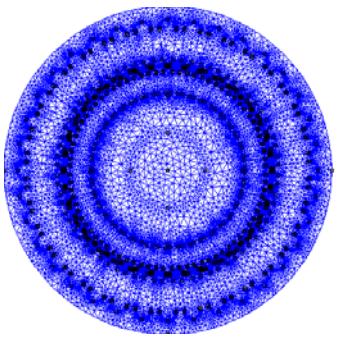

Figure 11. Mesh of finite elements

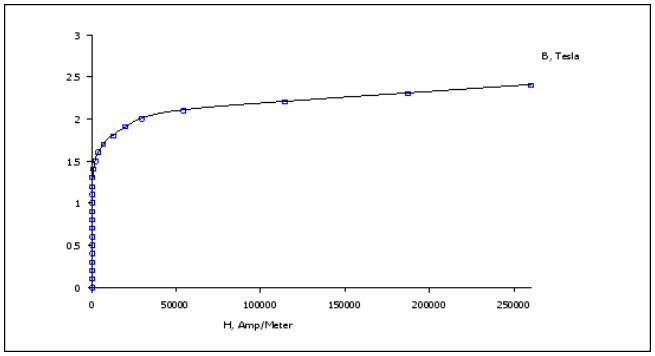


Figure 12. Characteristic of magnetization of iron core

The FEM model of the motor is derived for a time-harmonic analysis, i.e. the power supply of the stator winding with 50 Hz and currents in the rotor winding are freely induced due to the altering electromagnetic field from the stator winding. Fig. 8 presents the flux density distribution at a machine cross-section for no load and rated load. Fig. 9 presents the flux density distribution in the air gap of the motor for no load and rated load.

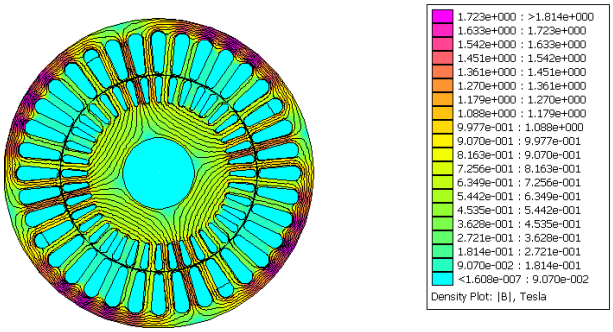


(a) no-load

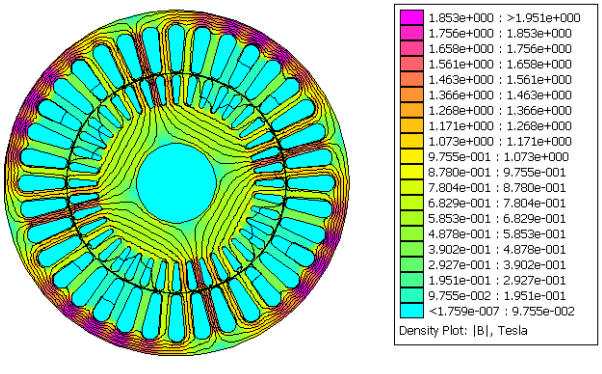


(b) rated load

Figure 13. Flux density distribution in machine cross-section

From the results presented in Fig. 8, the magnetic flux density distribution is within the limits of core saturation (Fig. 7). The air gap flux density in the induction motor is within the recommended values for this type of machine i.e. for 2p=4 (p is the number of pair of poles), the recommended value of air gap flux density is 0.65÷0.78 T [18].

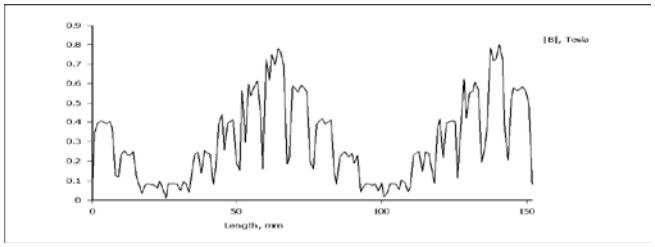


(a) no-load

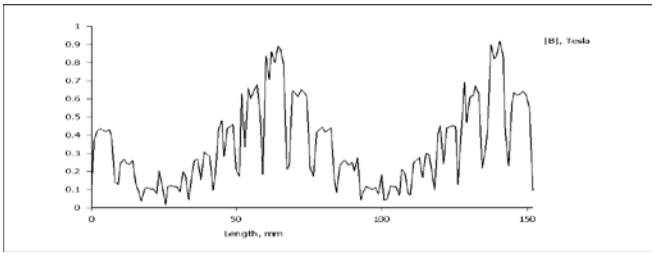


(b) rated load

Figure 14. Flux density distribution in motor air gap

The FEM discretization of the domain of the analyzed object produces a set of matrix differential equations. They are solved with the time decomposition method (TDM). The domain is decomposed along the time axis and all time steps are solved simultaneously instead of solving them time step by time step. The nonlinear matrix equations are linearized for each of the nonlinear iterations. As an output from the FEM model the value of torque for different operating modes- no load and rated load is obtained.

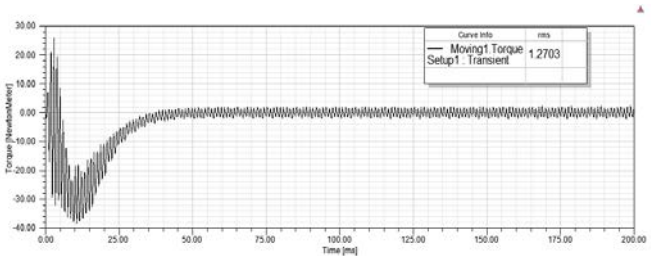


(a) no-load

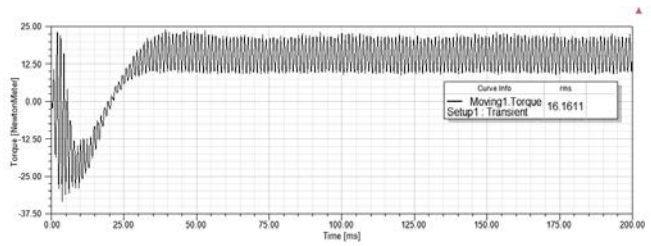


(b) rated load

Figure 15. Torque from the FEM model

Here, it must be noted that the results of the electromagnetic torque presented in Fig. 10 are obtained for one constant speed i.e. rated speed of 1362 rpm or no-load speed of 1499 rpm

within the whole time range 0÷200 ms (Fig.11). Therefore, the characteristics presented in Fig. 10 do not represent the transient characteristics of torque during motor acceleration from zero speed up to the rated or no-load speed. By using the TDM, the results presented in Fig. 10 are the calculated values of motor torque from the FEM motor model at one constant speed (rated or no-load speed) and they are used for verification of the results of the torque from the simulation and numerical model of the motor.

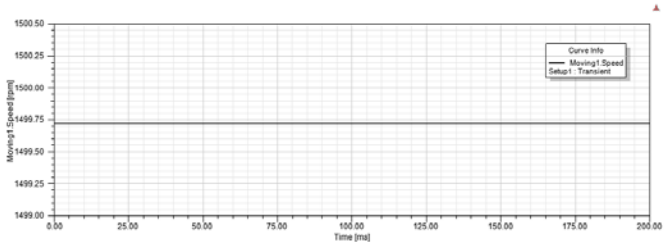


(a) no-load

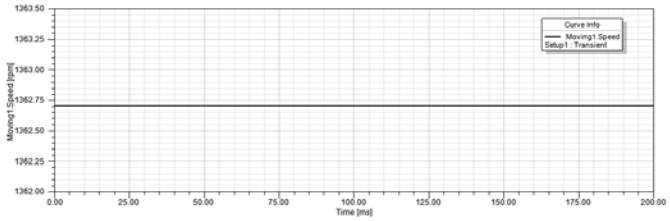


(b) rated load

Figure 16. Speed in the FEM model

## IV. PSIM MODEL

Different engineering software packages are available for the simulation of transient operating regimes of the electrical machines. In order to verify the results obtained from the SM and NM , the same motor is simulated in PSIM software for no load and rated load operation. The obtained results of current, speed and torque for no-load and rated load operation presented in Figs. 12 and 13 correspondingly.

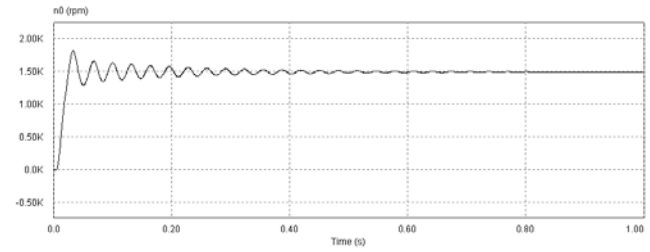


(a) no-load

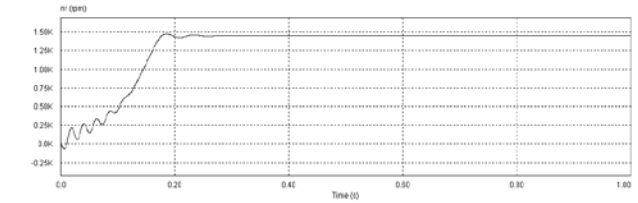


(a) rated load

Figure 17. Transient charactersitic of speed

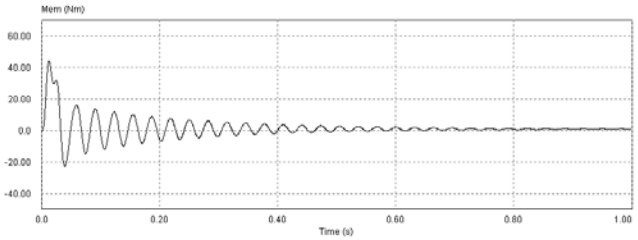


(a) no-load

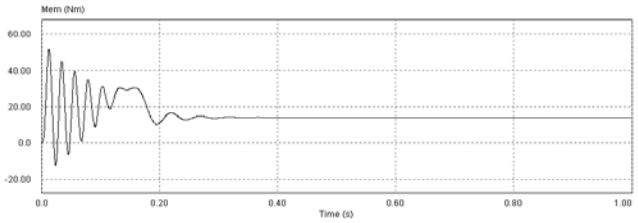


(b) rated load

Figure 18. Transient charatceristic of torque

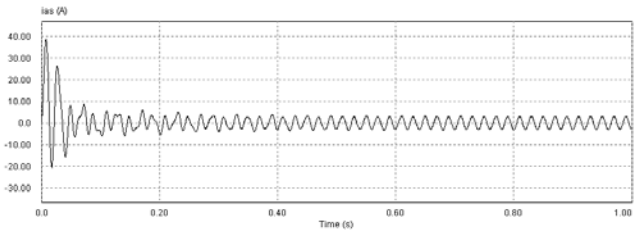


(a) no-load

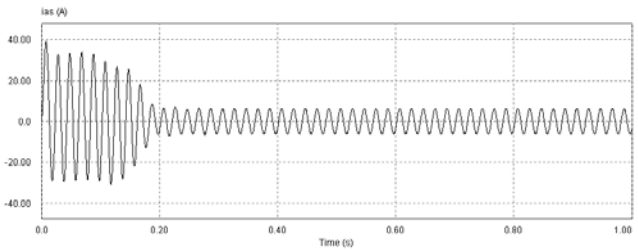


(a) rated load

Figure 19. Transient characteristic of current

## V. DISCUSSION OF THE RESULTS

The results obtained from the SM, NM, the FEM and PSIM motor model are compared and verified with the results from the analytical calculation and the experiment. The methodology of the analytical calculation of the electromagnetic torque and the experiment are explained and a comparison of the results from all the models is presented.

### *A. Analytical Calculation*

The electromagnetic torque of the motor is calculated from the T-equivalent circuit of the squirrel cage motor (Fig. 15).

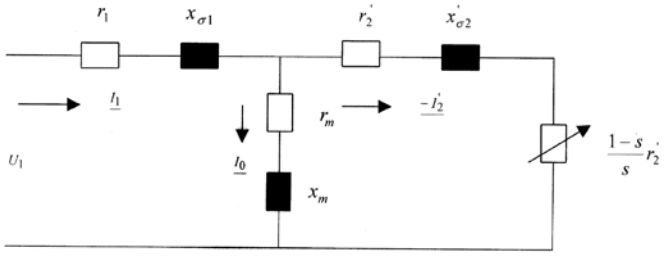


Figure 20. T-equivalent circuit

The stator current can be calculated from:

$$I_1 = \frac{U_1}{\underline{Z_e}} \tag{30}$$

The equivalent impedance is calculated from:

$$\underline{Z_e} = (r_1 + jx_{\sigma 1}) + \frac{jx_m\left(\frac{r_2'}{s} + jx_{\sigma 2}'\right)}{jx_m + \frac{r_2'}{s} + jx_{\sigma 2}'} \tag{31}$$

Where $r_1$ and $x_{\sigma 1}$ are the stator winding resistance and reactance, $x_m$ is the mutual reactance between the stator and rotor winding, and $r_2'$ and $x_{\sigma 2}'$ is the rotor winding resistance and reactance, referred to the stator side. $s$ is the slip calculated from:

$$s = (n_1 - n)/n_1 \tag{32}$$

where $n_1$ is the synchronous speed and n is the rotor speed. The power factor is calculated from:

$$\varphi = arctg[\mathrm{Im}(Z_e)/\mathrm{Re}(Z_e)] \tag{33}$$

The motor input power is:

$$P_1 = \sqrt{3} U_1 I_1 \cos\varphi \tag{34}$$

The electromagnetic power in the air gap is found from:

$$P_{em} = P_1 - P_{Fe} - P_{cu1} \tag{35}$$

$P_{Fe}$ are the iron losses. The copper losses are calculated from:

$$P_{cu1} = 3 r_1 I_1^2 \tag{36}$$

The electromagnetic torque is found from:

$$M_{em} = 9.55\, P_{em}/n_1 \tag{37}$$

Fig. 16 presents the electromagnetic torque for different motor slips in accordance with the analytical calculation. Furthermore, the complete set of motor characteristics (stator current $I_1$, efficiency factor η, power factor-cosφ, motor slip-s, input and output power $P_1$ and $P_2$, rotor speed-n, and motor output torque M) are calculated and presented in Table I.

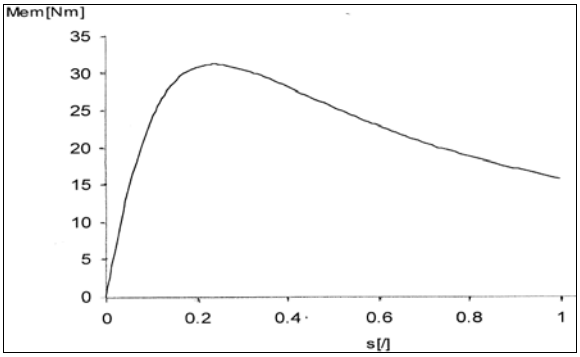


Figure 21. Electromagnetic torque at various motor slips

TABLE VI. MOTOR CHARACT. FROM THE ANALYT. CALCULATION

| $I_1$ (A) | η (/) | cosφ | s (/) | $P_1$ (W) | n (rpm) | M (Nm) | $P_2$ (W) |
|---|---|---|---|---|---|---|---|
| 2.17 | 0.128 | 0.1194 | 0.0006 | 171.32 | 1499.1 | 0.21 | 22 |
| 2.22 | 0.590 | 0.2547 | 0.0043 | 372.62 | 1493.5 | 1.48 | 220 |
| 2.32 | 0.732 | 0.3918 | 0.0086 | 600.87 | 1487.1 | 2.9 | 440 |
| 2.49 | 0.791 | 0.5078 | 0.0129 | 834.26 | 1480.5 | 4.34 | 660 |
| 2.71 | 0.82 | 0.6008 | 0.0175 | 1073.1 | 1473.7 | 5.79 | 880 |
| 2.97 | 0.835 | 0.6728 | 0.0223 | 1317.9 | 1466.6 | 7.25 | 1100 |
| 3.27 | 0.841 | 0.7274 | 0.0273 | 1569.3 | 1459.1 | 8.73 | 1320 |
| 3.60 | 0.843 | 0.7684 | 0.0325 | 1827.7 | 1451.3 | 10.23 | 1540 |
| 3.97 | 0.841 | 0.7989 | 0.0380 | 2094.1 | 1442.9 | 11.74 | 1760 |
| 4.37 | 0.836 | 0.8217 | 0.0439 | 2369.4 | 1434.2 | 13.28 | 1980 |
| 4.8 | 0.829 | 0.8384 | 0.0502 | 2654.8 | 1424.7 | 14.85 | 2200 |

Two typical operating regimes of the machine no load and rated load are highlighted in Table I. The current of 2.22 A represents the no-load operating regime and the current of 4.37 A is obtained for rated load operation.

*B. Experiment*

The three-phase squirrel cage motor was tested in the faculty laboratory at no load and for the rated load operation. During the no-load test, the motor is accelerated almost to the synchronous speed and the motor input power $P_0$, as well as the no-load current $I_0$ and power factor $\cos\varphi_0$ are measured. The measurements are done for several supply voltages. The measurement for 220 V is presented in Table II, as this measurement actually represents the no-load operation of the motor. The loading of the motor up to the rated operating point is done with a mechanical break and two dynamometers. The motor is gradually loaded up to the rated current. Voltage is kept at 220 V. The output power $P_2$ is calculated from:

$$P_2 = P_1 - (P_k + P_{Fe,md}) \tag{38}$$

where $P_k$ are short circuit losses (measured from the short circuit experiment). $P_1$ is the motor input power from the

network. $P_{Fe,md}$ are iron and mechanical losses due to friction. They are calculated from the no-load experiment:

$$P_{Fe,md} = P_0 - 3r_1 I_0^2 \tag{39}$$

The output torque on the rotor shaft is:

$$M = 9.55 \cdot (P_2 / n) \tag{40}$$

The results from the experiments (no load and rated load) are presented in Table II.

TABLE VII. DATA FROM EXPERIMENT

| rated load | | | | | | | |
|---|---|---|---|---|---|---|---|
| ***U* (V)** | ***I* (A)** | ***P*k (W)** | ***P*Fe, md (W)** | ***P*1 (W)** | ***P*2 (W)** | ***M*n (Nm)** | ***n*n (rpm)** |
| 220 | 4.9 | 417 | 147.99 | 2510 | 1945.01 | 13.17 | 1410 |
| **no-load** | | | | | | | |
| ***U*0 (V)** | ***I*0 (A)** | ***P*0 (W)** | ***P*Fe, md (W)** | ***M*o (Nm)** | ***n*0 (rpm)** | | |
| 220 | 2.37 | 196 | 147.99 | 1.25 | 1495 | | |

*C. Comparison of Results and Discussion*

Fig. 1 presents the transient characteristic of torque for no load and rated load in the simulation model. For no-load operation, after the torque transients are suppressed, the torque reaches the no-load torque of 1.3 Nm. For the rated load after the motor acceleration has finished, the torque reaches the steady state value of 15.4 Nm. In Fig. 2, the motor accelerates at no load very quickly for less than 0.1 s, and reaches the steady-state speed of 1498 rpm or 313 rad/s. As for the rated load acceleration, acceleration lasts longer, approximately 0.2 s and then the motor reaches the steady state operation of 1433 rpm or 300 rad/s. Fig. 3 presents the transient characteristic of the stator current in the simulation model for no-load and rated load operation. At no load, the motor accelerates with a starting current, multiple times the rated current, and reaches the steady-state no-load current of 2 A (rms value). At rated load, after the motor starting has finished, the current reaches the steady state value of rated current of 4.3 A (rms value).

The motor behavior in the numerical model is similar to the simulation model. In Fig. 4, the motor at no-load operating mode accelerates up to 313 rad/s and at rated load up to 300 rad/s or 1433 rpm. The acceleration time in both cases, at no load and rated load, is similar to the acceleration time of the motor in the simulation model. Fig. 5 presents the transient characteristic of torque for no load and rated load. At no load, after the acceleration has finished, the motor reaches the no-load torque of 2.5 Nm, although, in the numerical model, the torque transients are more emphasized. At rated load, the steady state value of rated torque is 16.6 Nm. The comparison of the results from both motor models - the simulation and the numerical is done on the basis of the obtained values of the torque and speed of the motor after the transients are suppressed and the motor reaches the stable value of speed or torque.

The FEM model of the motor provides the characteristics of torque at no load and rated load (Fig. 9) for one constant speed within the simulated time interval i.e. the no load or rated speed . At no load, the output torque is 1.27 Nm and the rated torque is 16.1 Nm. Since the presented characteristics of torque from the FEM model (Fig.10) are simulated for one constant speed within the whole time interval (Fig. 11), they do not represent the transient characteristics of torque at motor acceleration from zero to the no-load or the rated speed. They are used for the verification of the obtained values of the torque from the transient characteristics in the simulation and numerical models, after all transients are suppressed. Also, the FEM model is a useful tool in estimation of magnetic core saturation. In accordance with the obtained results of the magnetic flux density (Fig. 8), the flux density is within the limit of core saturation (Fig. 7) and within the recommended values of flux density in the air gap of the four pole induction machine (Fig. 9). Further more FEM model of the motor includes the nonlinearity of magnetic core saturation since this was not taken into consideration in the simulation and the numerical motor model.

Motor is modeled in PSIM software in order transient characteristics of torque, speed and current from simulation and numerical model to be verified. Comparison of results from Figs 2, 4 and 12 verifies the similarity of the transient characteristics of speed from all three models (simulation, numerical and PSIM) with respect to the time of acceleration as well as the final steady state value of speed at no load and rated load. Similar behavior is observed from the comparison of characteristics of torque (Figs. 1, 5 and 13) as well as from the comparison of characteristics of current (Figs. 3 and 14). More detailed comparison of the obtained results is presented in Table IV.

In both transient models, the same motor parameters from the motor nameplate are used, and they are presented in Table III. In Table III, the rated torque and the no-load torque are calculated from (40) by replacing the adequate rated power and rated speed, i.e. no-load losses and no-load speed.

TABLE VIII. MOTOR DATA FROM THE NAMEPLATE /PRODUCER

| Parameter | Value |
|---|---|
| nominal power- Pn | 2.2 kW |
| number of poles p | 2p=4 |
| nominal voltage Δ/Y | 220/380 V |
| nominal current Δ/Y | 8.7/5 A |
| power factor-cosφ | 0.81 |
| nominal speed-$n_n$ | 1410 rpm |
| rated torque $M_n$ | 14,9 Nm |
| no-load losses $P_0$ | 170 W |
| no-load torque $M_0$ | 1,085 Nm |

The verification of all the theoretical models (the numerical, the simulation, the FEM and the PSIM) is done with analytical calculations and measurements. Where available, all results are compared with the data obtained from the motor producer [19]. This comparison is presented in Table IV. In Table IV, subscript “0” denotes no-load operation and “n” denotes rated-load operation. In addition, it should be noted that the speed in Table IV is in rpm, derived from the speed in rad/s in Figs. 2 and 4. The rms values of currents are presented in Table IV. The results from the FEM model are read out

within the last time interval of twenty five milliseconds in Fig. 10, after the torque characteristics and the calculation of torque in the FEM model has reached the relatively stable value.

TABLE IX. COMPARISON OF RESULTS

| | SM | NM | FEM | PSIM | Anal cal. | Exp. | Prod. |
|---|---|---|---|---|---|---|---|
| $I_0$ (A) | 2 | / | / | 2.1 | 2.2 | 2.37 | 2.4 |
| $I_n$ (A) | 4.3 | / | / | 4.6 | 4.4 | 4.9 | 5 |
| $M_0$ (Nm) | 1.3 | 2.5 | 1.2 | 1.5 | 1.48 | 1.25 | 1.1 |
| $M_n$ (Nm) | 15.4 | 16.6 | 16.1 | 14.5 | 13.3 | 13.2 | 14.9 |
| $n_0$ (rpm) | 1498 | 1498 | 1499 | 1499 | 1493 | 1495 | 1495 |
| $n_n$ (rpm) | 1430 | 1433 | 1362 | 1440 | 1434 | 1410 | 1410 |

From the comparison of the results presented in Table IV it is evident that there is some difference in the torque from the simulation, numerical and the FEM model in comparison with the torque obtained from the analytical calculation, experiment and producer data. In the case of the experiment and producer data, the torque presented in Table IV is a torque on the motor shaft, which differs from the electromagnetic torque in the air gap, calculated by SN, NM and FEM due to friction and certain stray losses, which decrease the output torque in comparison with the air gap torque. The analytical calculation does not take into account time varying inductances, which can cause some differences in the results.

## VI. CONCLUSION

The estimation of the operation of the induction motor at various operating modes is an important engineering task. Often, simulation models are used for the evaluation of various dynamic regimes of the motor operation. They provide useful information in terms of motor coupling with the load and motor behavior during start up and steady state operation. The paper presents two different transient models of squirrel cage motor derived from the two sets of differential equations, which are solved in Simulink and in Matlab. As an output from both models, the transient characteristics of speed and torque for various operating modes are obtained. The motor is modeled in the FEM and PSIM software as well. The FEM model allows the magnetic flux density distribution to be calculated, as well as the torque characteristics for one constant speed corresponding to the motor operating regime. All three models from Simulink, Matlab and FEM are verified by analytical calculation, experiment, PSIM results and available data from the motor producer. The comparison of the results verifies the derived transient models of the motor as sufficiently accurate. The derived models are universal and can be applied on any asynchronous motor, by simple replacement of the adequate motor parameters and load type. However, the nonlinearity of the magnetic core saturation in modeling of both dynamic models was not taken into consideration. This opens a new perspective of further modification and extension of the derived models. In addition, motor optimization is another filed of possible extension of motor models, subject to author's further research.

## REFERENCES


[8] P. Miljanić: Tesla's Polyphase System and Induction Motor, Serbian Journal of Electrical engineering, Vol. 3, No. 2, November 2006, pp. 121 – 130.

[9] G. Rafajlovski, M. Digalovski, " PWM Inverter Dead Time impact on Vector Control System," International Journal on Information Technologies & Security, vol. 7, no. 4, pp. 73 – 84, 2015.

[10] D-C Popa, B. Vărăticeanu, D. Fodorean, P. Minciunescu, C. Martis, "High Speed Induction Motor used in Electrical Vehicles, Electrotehnica, Electronica, Automatica (EEA)", vol. 64, no.3, pp. 5 – 11, 2016.

[11] M.A. Jirdehi, A. Rezaei, "Parameters Estimation of Squirrel-Cage Induction Motors using ANN and ANFIS", Alexandria Engineering Journal, vol. 55, no. 1, pp. 357 – 368, March 2016.

[12] K. Makowski, M. J. Wilk, "Experimental Verification of Field-Circuit Model of a Single-Phase Capacitr Induction Motor", Prezglad Electrotechniczny, vol. 88, no. 7B, pp. 116 – 118, 2012.

[13] R. Renkevičiené, A. Baškys, A. Petrovas, "Model for Simulation of Dynamic Characteristics of the System Frequency Converter-AC Induction Motor", Elektronika ir Electrotehnika, vol. 82, no. 2, 2008, pp. 65 – 68, 2008.

[14] S. A. Fellag, "Steady State and Dynamic Evaluation of Electrical Shaft System, Journal of Electrical Engineering", vol. 61, no. 5, pp. 277 – 281, 2010.

[15] M. Boucherma, M. Y. Kaikaa, A. Khezzar, "Park Model of Squirrel Cage Induction Machine including Space Harmonics Effects", Journal of Electrical Engineering, vol. 57, no. 4, pp. 193 – 199, , 2006.

[16] S. I. Deaconu, M. Topor, G. N. Popa, D. Bistrian, "Experimental Study and Comparative Analysis of Transients of Induction Motor with Soft Starter Startup", Advances in Electrical and Computer Engineering, Vol. 10, No. 3, pp. 27 – 33, 2010.

[17] Lj. S. Peric, S. N. Vukosavic, "High Performance Digital Current Control in Three Phase Electrical Drives, Facta Universitatis", Series: Electronics and Energetics, vol. 29, no. 4, pp. 653– 674, 2016.

[18] A. Alaeddini, A. Darabi, H. Tahanian, "Influence of Various Structural Factors of Claw Pole Transverse Flux Permanent Magnet Machines on Internal Voltage using Finite Element Analysis", Serbian Journal of Electric Engineering, vol. 12, no. 2, pp. 129– 143, June 2015.

[19] Y-L. He, M-Q. Ke, G-J. Tang, H-C. Jiang, X-H. Yuan, "Analysis and Simulation on the Effect of Rotor Interturn Short Circuit on Magnetic Flux Density of Turbo-Generator", Journal of Electrical Engineering, Vol. 67, No. 5, 2016, pp. 323– 333.

[20] M. Ahmadi, J. Poshtan, M. Poshtan, "Modeling Squirrel Cage Induction Motors using Finite Element Method", IEEE International Conference on Intelligent Control Automatic Detection and High-End Equipment, China, pp. 186 – 191, 2012.

[21] T. Vaimann, A. Belahcen, A. Kallaste, "Changing of Magnetic Flux Density Distribution in a Squirrel-Cage Induction Motor with Broken Rotor Bars", Elektronika ir Elektrotechnika, vol. 20, no. 7, pp. 11 – 14, 2014.

[22] V. P. Sakthivel, S. Subramanian, "On-site Efficiency Evaluation of Three-Phase Induction Motor based on Particle Swarm Optimization", Energy, vol. 36, no. 3, pp. 1713 – 1720, March 2011.

[23] G. Tamás, P. A. Attila, B.K. Ágoston, "Optimization of a Three-Phase Induction Machine using Genetic Algorithm, 30th micro CAD International Multidisciplinary Conference", University of Miskolc, Hungary, pp. 1 – 5, April 2016.

[24] A. G. Yetgin, M. Turan: Efficiency Improvement in Induction Motor by Slitted Tooth Core Design: Tehnical Gazzete, Vol. 24, No. 5, 2017, pp. 1291– 1296.

[25] I. Boldea, S. A. Nasar: The Induction Machines Deign Handbook, CRC Press, USA, 2010.

[26] Končar –MES, d.d.: Three-phase squirrel cage induction motors, Catalogue.